Heliyon 5 (2019) e02426

Contents lists available at ScienceDirect

Heliyon

journal homepage: www.heliyon.com

Synthesis, and molecular modeling of bis(3-(piperazine-1-yl)propyl) tungstate (BPPT) nanoparticles, and its first catalytic application for one-pot synthesis of 4*H*-chromene derivatives

Khalil Eskandari [a], Yaghoub Pourshojaei [a,b,*], Fatemeh Haghani [a], Mahnaz Shabani [a], Ali Asadipour [a]

[a] *Department of Medicinal Chemistry, Faculty of Pharmacy & Pharmaceutics Research Center, Institute of Neuropharmacology, Kerman University of Medical Sciences, Kerman, Iran*

[b] *Neuroscience Research Center, Institute of Neuropharmacology, Kerman University of Medical Sciences, Kerman, Iran*

ARTICLE INFO

Keywords:
Organic chemistry
Bis(3-(piperazin-1-yl)propyl)tungstate
Molecular modeling
Recyclable catalyst
4H-chromens
Green protocol

ABSTRACT

A novel, nano-sized, bis(3-(piperazine-1-yl)propyl)tungstate (BPPT) is introduced as an efficient and reusable organometallic catalyst which is considered as a heterogeneous Bronsted-Lowry base and applied successfully for one-pot synthesis of methyl 2-amino-4-aryl substituted-4*H*-chromene derivatives with good to excellent yields. BPPT has been prepared via a two-step route from natrium tungstate salt. At first, the oxygens of Na_2WO_4 react with 1-bromo-3-chloropropane via nucleophilic substitution to produce bis(3-choloro propyl)tungstate. Then nucleophilic substitution of piperazine with chlorines produced bis(3-(piperazine-1-yl)propyl) tungstate. Bis(3-(piperazine-1-yl)propyl) tungstate, which was called BPPT, characterized by fourier transform infrared spectroscopy (FT-IR), X-ray diffraction (XRD), thermal gravimetric analysis (TGA), transmission electron microscopy (TEM) and scanning electron microscope (SEM). The catalyst is heterogeneous, green and recyclable. It is a thermally stable and its handling is easy. Its catalytic activity is very high and leads to the production of 4*H*-pyran derivatives with good to excellent yields in short reaction times. Furthermore, molecular modeling studies and ADMETox prediction revealed that not only it can inhibit acetylcholinesterase enzyme and act as an anti-Alzheimer agent but also has no variation from Lipinski's rule of five and can be a good candidate as anti-Alzheimer agents. These above-mentioned facts can be countered as advantages of the current protocol.

1. Introduction

During last decades, many efforts have been made to the synthesis and development of supported heterogeneous catalysts that they are often organometallic (Eskandari et al., 2014; Karami et al., 2013d; Zhai et al., 2018). Although sometimes it has been observed that homogenous catalysts have been used for the synthesis of a wide range of organic and biologically active compounds (Antonangelo et al., 2017; Fogeron et al., 2018), but they are minimally recyclable, difficulty to handle and storage, hazardous for environment, and also most of them are expensive, therefore, are not desirable for industrial applications (Fukutake et al., 2018). As a result, one of the important approaches for overcoming to the above-countered problems is the preparation and application of heterogeneous supported catalysts (Eskandari et al., 2018a; Ye et al., 2018). Heterogeneous supported catalysts generally have numerous benefits such as good catalytic performance, recyclability, environment safety, high stability, being cheap, and simple handling (Li et al., 2018b). So synthesis and characterization of heterogeneous supported catalysts and their applications in the synthesis of organic and heterocyclic compounds have recently been attracted the interest of chemists and industrialism (Alzeer and MacKenzie, 2018). Aliphatic amines such as piperidine or piperazine due to the presence of delocalized electrons on nitrogen are known as organic base, which are used as conventional active catalyst for the synthesis of organic compounds (Habibi et al., 2012; Karami et al., 2012), but they have some disadvantages such as what mentioned above for homogeneous catalysts along with they are mostly soluble in organic solvents and their separation from homogeneous reaction mixtures require neutralization by acidic conditions, which lead to worthless ammonium salt (Rahmani-Nezhad et al., 2015; Saidi et al., 2009). Harmful effects of acidic work-ups can be removed by immobilization of

* Corresponding author.
E-mail address: y.pourshoja@kmu.ac.ir (Y. Pourshojaei).

https://doi.org/10.1016/j.heliyon.2019.e02426
Received 12 December 2018; Received in revised form 26 August 2019; Accepted 2 September 2019
2405-8440/© 2019 Published by Elsevier Ltd. This is an open access article under the CC BY-NC-ND license (http://creativecommons.org/licenses/by-nc-nd/4.0/).

aliphatic amines for example piperazine onto solid supports to obtain heterogeneous catalysts (Gupta et al., 2015). To profit from this technology, to date, various clean materials such as graphene (oxide) sheets (Eskandari and Karami, 2016; Khalili and Dehghani, 2016), silica or mesoporous silica (Pourshojaei et al., 2018b; Uruş et al., 2018), Fe_3O_4 nanoparticles (Maleki et al., 2014), and dendrimer (Pullur Anil Kumar, 2010), have been using as support for preparation of new heterogeneous base catalysts to overcome the problems related to the homogeneous base catalysts.

Tungsten is an important element in chemistry and compounds containing tungsten have wide range of applications not only in chemical laboratories but also in various fields of industries such as catalysts (Kocięcka et al., 2018), optical fibers (Liu et al., 2018b), and sensors (Waghmare et al., 2018), and electrochromic applications (Li et al., 2018a). Meanwhile, tungstate supported catalysts for the synthesis of organic compounds have also been recently applied successfully (Farahi et al., 2017; Karami et al., 2013a, 2013b).

Chromene and its derivatives are very important *O*-containing heterocyclic compounds in medicinal chemistry. They have shown so many biological activities including reducing the risk of cardiovascular diseases (Aune et al., 2018), anti-allergic (Chen et al., 2018), anti-microbial (Chen et al., 2018), analgesic (Chen et al., 2018), anti-parkinsonian (Banoth et al., 2018), anti-human immune deficiency virus (HIV) (Banoth et al., 2018), antibacterial (Lee et al., 2018), anti-tumor (Banoth et al., 2018) anti-diabetic (Davidson et al., 2018) and anti-inflammatory (Davidson et al., 2018). Also, some of them have recognized as non-nucleoside reverse transcriptase inhibitor (Chenera et al., 1993), and act in the role of an enzyme that can catalyze chemical reactions (Engleder and Pichler, 2018). Taking a brief look at Fig. 1 which shows some significant biological active compounds containing chromene framework, can more disclosed the highly importance of this family of heterocyclic compounds (Aune et al., 2018; Chenera et al., 1993; Davidson et al., 2018; Engleder and Pichler, 2018; Lee et al., 2018).

In regard to the importance of chromene and its derivatives (Maleki, 2016a, 2016b; Maleki and Sheikh, 2015a, 2015b) and also the significant role of supported heterogeneous catalysts in chemical syntheses and industries (Alinezhad et al., 2019; Brückner et al., 2009; Chafran et al., 2019; Maleki et al., 2015), herein we wish to report a nano-sized novel heterogeneous supported Brönsted base as an efficient catalyst which was successfully applied to synthesis of new 4*H*-chromene derivatives. We called this newly prepared nanocatalyst bis(3-(piperazine-1-yl)propyl) tungstate (BPPT) that was prepared in an alternative two-step route from sodium tungstate (**1**), 1-bromo-3-chloro-propane (**2**), and piperazine (**4**) (Scheme 1).

In continuous of our research on the synthesis of biological active compounds (Eskandari et al., 2018b; Mehrabi et al., 2017), heterogeneous catalysts (Eskandari and Karami, 2018; Pourshojaei et al., 2018a), and a wide range of organic and heterocyclic compounds (Asadipour et al., 2018, 2017), in this work we wish to report preparation and characterization of BPPT, for the first time, and its performance as a nano-sized heterogeneous catalyst in a one-pot three-component combinatorial reaction via a green procedure. It found that BPPT as a heterogeneous Brønsted base can successfully catalyze Knoevenagel condensation, Michael addition and intramolecular cyclization reaction between methyl cyanoacetate (**5**), a wide range of aryl aldehydes **6**, and dimedone (**7**) to afford 4-aryl substituted 4*H*-chromene derivatives **8** in good to excellent yields (Scheme 2).

2. Results and discussion

With reference to green chemistry aspects, it is very important that chemical reactions have been run under green conditions. Hence the use of eco-friendly catalysts and solvents are inevitable. Also, industrially and economic point of view it is very important that applied catalysts in chemical reactions to be highly efficient and recyclable. Accordingly, so many attempts have been taken place so far by chemists to the preparation of green, highly efficient and recyclable catalysts and their applications in organic syntheses (Eskandari et al., 2014; Karami et al., 2013d; Zhai et al., 2018). Based on above, herein we wish to report a novel, highly efficient and eco-friendly nano-catalyst and its first application in the synthesis of 4*H*-chromene derivatives as highly efficient, and recyclable basic catalyst. By a brief looking at Scheme 1, it is leveled

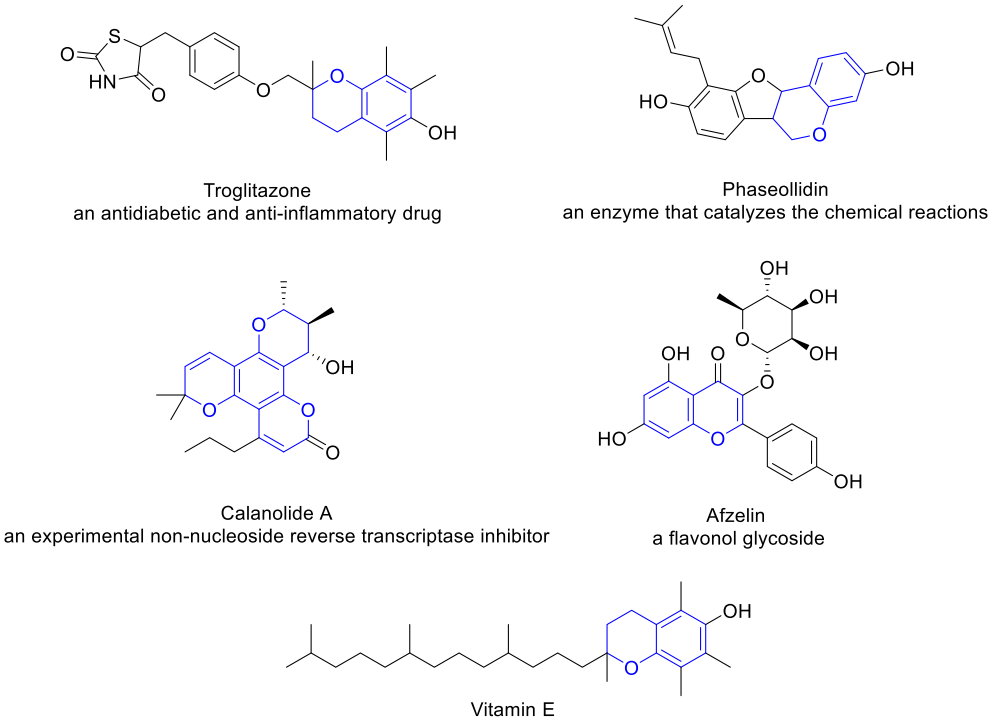

Fig. 1. Selected significant biologically active compounds containing a chromene framework.

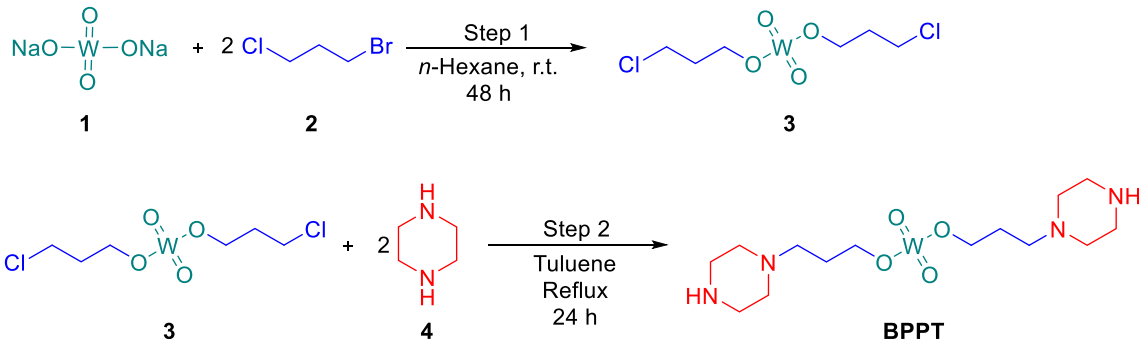

Scheme 1. Alternative two-step route to the preparation of BPPT.

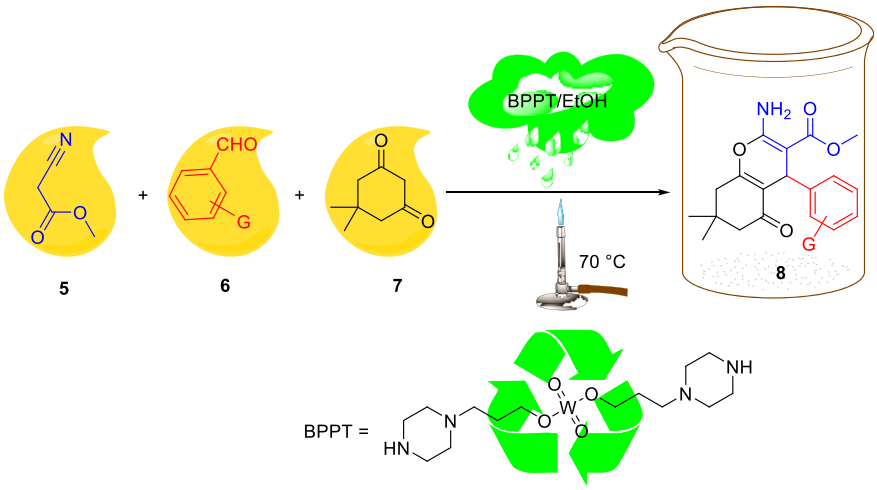

Scheme 2. BPPT-catalyzed green synthesis of 4*H*-chromene derivatives.

that newly prepared catalyst which was called BPPT was synthesized in an alternative two-step route from sodium tungstate **1**, 1-bromo-3-chloropropane **2** and piperazine **4**. As can be seen from Scheme 1, in the first step, bis(3-chloropropyl)tungstate **3** is formed from the reaction between sodium tungstate **1** and 1-bromo-3-chloropropane **2**, then in the second step, 1-bromo-3-chloropropane 2 is treated with piperazine 4 to afford bis(3-(piperazine-1-yl)propyl) tungstate nanoparticles (BPPT NPs). It is noteworthy to consider that the reaction procedure is clean and easy. BPPT NPs was characterized by FT-IR spectra, scanning electron microscopy (SEM), transmission electron microscopy (TEM) and atomic

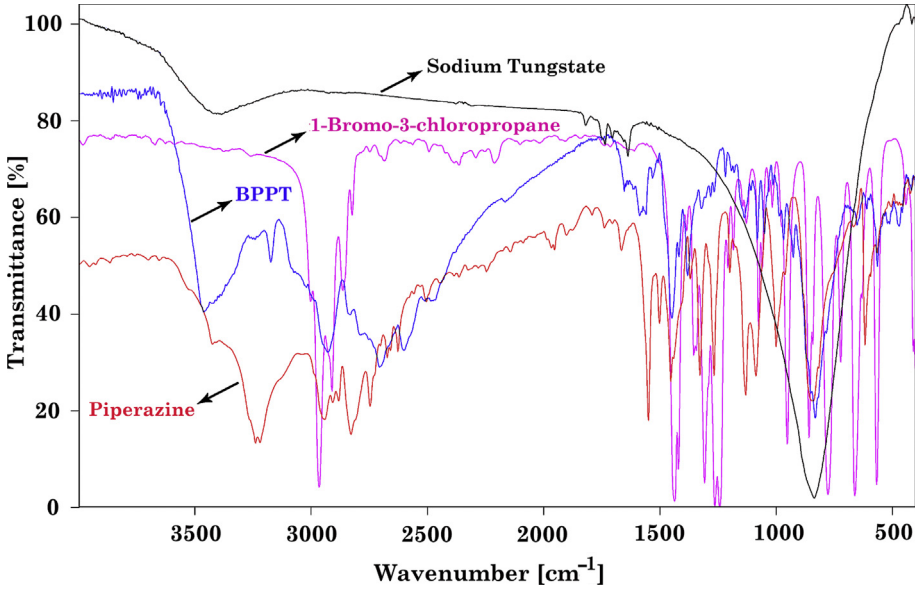

Fig. 2. Comparable FT-IR spectra of anhydrous sodium tungstate, 1-bromo-3-chloropropane, piperazine, and BPPT NPs.

absorption.

2.1. Characterization and application of catalyst

Fig. 2 shows mixing FT-IR spectra of the anhydrous sodium tungstate 1, 1-bromo-3-chloropropane 2, piperazine 4, and BPPT NPs. By a brief looking at the spectrum of BPPT NPs and its comparison with the spectra of starting materials, it is obviously revealed that both 1-bromo-3-chloropropane and piperazine have joined to tungstate core. For instance, the spectrum of BPPT NPs shows significant peaks of tungstate group (appeared at 3462 and 836 cm^{-1}), important peaks of the propyl group appeared at 2927 cm^{-1} (CH stretch) and 1448 cm^{-1} (CH bend), and distinguished peaks of piperazine appeared at 3173 cm^{-1} and 2706 cm^{-1}. Also, the investigation of the catalyst by atomic absorption spectroscopy showed the existence of tungsten in catalyst structure that is in agreement with appeared peaks of tungstate group in FT-IR spectroscopy.

The scanning electron microscope (SEM) image of as-prepared BPPT NPs shows the bis(3-(piperazine-1-yl)propyl) tungstate nanoparticles have a diameter of around 30 nm (Fig. 3). Furthermore, the transmission electron microscopy (TEM) image of BPPT NPs was taken to more investigate of BPPT NPs morphology (Fig. 4). The TEM image of BPPT NPs clearly disclosed the BPPT NPs have a diameter size of about 30 nm.

Also, to support the stability of BPPT NPs at high temperatures, thermogravimetric (TGA) analysis was carried out (Fig. 5). From the obtained TGA curve, it was revealed that weight percent remains constant till 100 °C. Therefore, it is concluded that the BPPT NPs is stable in temperatures below 100 °C.

After characterization of the catalyst, with respect to the importance of using novel green and recyclable heterogeneous catalyst in chemical synthesis, herein, we decided to use and investigate the effectiveness of BPPT NPs in the synthesis of 4*H*-chromene derivatives. In continues of our research studies on the synthesis and application of nanocatalysts in organic syntheses (Eskandari and Karami, 2018; Karami et al., 2013c; Pourshojaei et al., 2018b), we found that BPPT NPs can act as a potent, green and recyclable catalyst in an alternative two-step reactions that is Knoevenagel condensation and Michael reaction between methyl cyanoacetate (**5**), aryl aldehydes **6** and dimedone (**7**) to afford chromene derivatives **8** in good to excellent yields (Scheme 2).

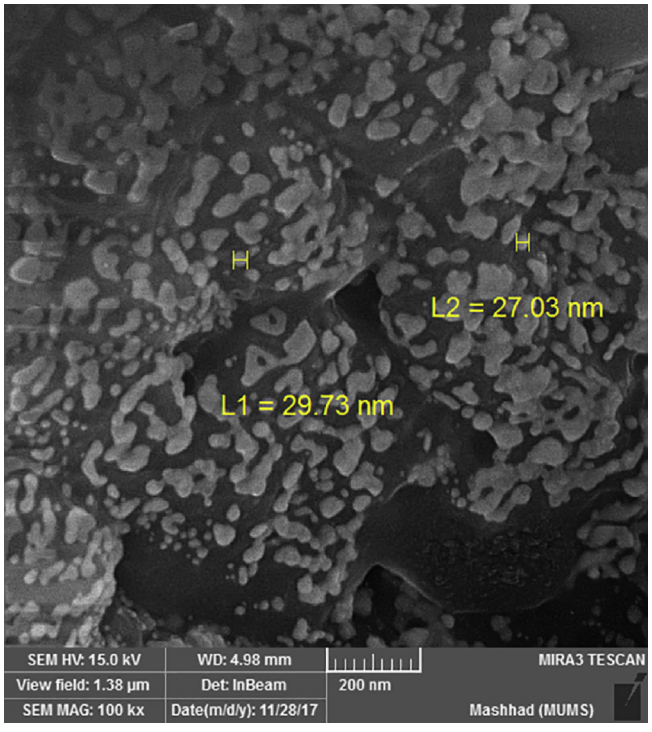

Fig. 3. The SEM image of BPPT NPs.

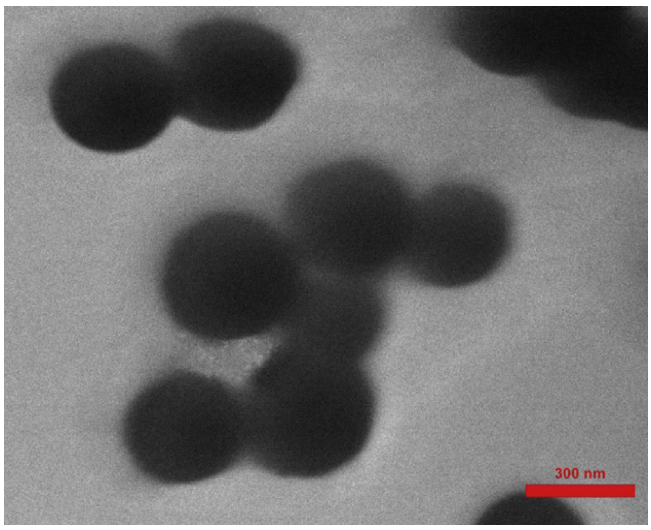

Fig. 4. The TEM image of BPPT NPs.

In this protocol, it was found that BPPT NPs has significant advantages including being eco-friendly, recyclability, high thermal stability, and also high efficiency.

Before start reaction runs, it was necessary to find optimum conditions for reaction progress. For this purpose, compound **8d** was selected as a model. Loading model reaction in various solvents including dichloromethane, chloroform, toluene, water, DMF, acetonitrile, THF, methanol, and ethanol disclosed that reaction progress was faster in ethanol than others and caused to obtain the product with the highest yield. Next, the effect of temperature on reaction progress was assessed, and it was found that 70 °C is the best temperature to achieve the product with the highest yield. In the next step, other same catalysts were applied to the model reaction and compared with BPPT NPs. From obtained results which are summarized in Table 1, it is understood that BPPT NPs is the most effective catalyst in the synthesis of the target compound.

In the next step, the effect of catalyst amount on the model reaction was examined that obtained results are summarized in Table 2. By a closer looking at Table 2, it is found that the use of the catalyst in this reaction is inevitable and the best amount of required catalyst which leads to obtaining target product with the highest yield is 5 mol%.

After achieving optimal conditions, in order to examine the generality of the protocol, the reaction was loaded with methyl cyanoacetate (**5**), a wide range of aryl aldehydes **6** and dimedone (**7**) in the presence of 5 mol % BPPT NPs as basic catalyst and the results were summarized in Table 3 (Guo et al., 2013; Li et al., 2006; Patra and Mahapatra, 2010; Rong et al., 2006; Wang et al., 2003).

For confirmation of obtained products **8**, their chemical structures were characterized by FT-IR, ^{1}H NMR, ^{13}C NMR spectroscopies, and also elemental analyses (Figs. S1–S30, supplementary materials). For example, the ^{1}H NMR spectrum of **8d** (Fig. S10) indicates an identifiable singlet at 7.56 ppm related to NH_2 group, multiple peaks around 7.46 are correlated with four protons of the aromatic ring, two doublets appeared in 7.07 and 6.86 ppm are corresponded for four protons of the other 1,4-substituted phenyl ring. Three singlets appeared at 5.03, 4.49, and 3.52 ppm are corresponded for two protons of OCH_2 group, one proton of methine group, and three protons of OCH_3 group respectively. The four doublets in chemical shifts of 2.55, 2.46, 2.27, and 2.07, each for one proton, are related to four diastereotopic protons of cyclohexenone fragment. Also, the six protons related to two methyls groups ($2\times CH_3$) are appeared at 1.05 and 0.90 ppm as two singlets. ^{13}CNMR spectrum of **8d** (Fig. S11) also shows 21 distinct resonances in agreement with the proposed structure. Furthermore, FT-IR spectrum of **8d** (Fig. S12) clearly disclosed the bonds correlated to NH_2 and carbonyl groups at 3431,

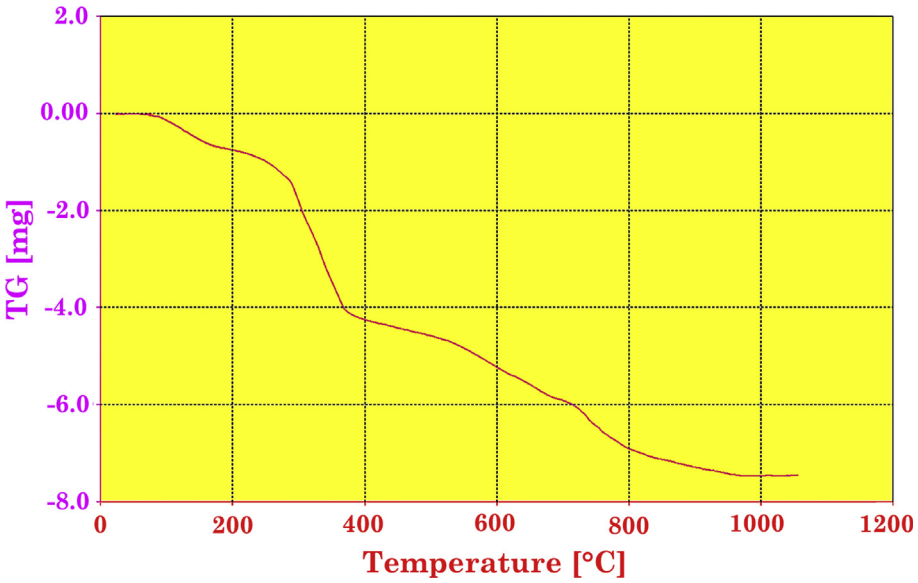

Fig. 5. The TGA analysis of BPPT NPs.

Table 1
Effect of different catalysts on a model reaction.[a]

Entry	Catalyst	Time	Yield[b]
1	$FeCl_3.6H_2O$	90	68
2	$Y(NO_3).6H_2O$	80	75
3	$CuSO_4.5H_2O$	80	65
4	*p*-TSA	80	70
5	Na_2HPO_4	60	81
6	K_2CO_3	60	82
7	$Na_2WO_4.2H_2O$	60	84
8	Piperidine	60	80
9	BPPT NPs	40	95

[a] Reaction conditions: catalyst (5 mol%), methyl cyanoacetate (1.25 mmol), 4-((4-chlorobenzyl)oxy)benzaldehyde (1 mmol), dimedone (1 mmol), EtOH (8 mL), 70 °C.
[b] Refers to isolated yields.

Table 2
Optimization of catalyst amount for the model reaction.[a]

Entry	Catalyst (mol%)	Time (min)	Yield[b] (%)
1	—	90	Trace
2	1	60	50
3	2	60	88
4	3	40	90
5	4	40	93
6	5	40	95
7	6	40	95
8	7	40	93

[a] Reaction conditions: methyl cyanoacetate (1.25 mmol), 4-((4-chlorobenzyl)oxy)benzaldehyde (1 mmol), dimedone (1 mmol), EtOH (8 mL), 70 °C.
[b] Refers to isolated yields.

3315, 1688 and 1666 cm^{-1} respectively compatible with proposed structures.

2.2. Recyclability study of BPPT NPs

Despite being effective and requiring a small amount of catalyst, the capability of catalyst to reuse is the other advantage of BPPT NPs. In this content, we wish to examine the recyclability of catalyst on model reaction. For this purpose model reaction was loaded using 5 mol% of fresh, once, twice, three-, four- and five-time used BPPT NPs. For reusing catalyst in another cycle, it should be separated from the reaction mixture by filtering and washing with THF, drying at 80 °C for 1 h, and then can reuse in further cycles. The results showed that BPPT NPs is able to reuse in further cycles (up to five times) besides its first use without a remarkable miss of activity (Fig. 7).

In an additional investigation, the FT-IR spectra of the catalyst before and after use as an appropriate comprehensive study for recycled catalyst were compared (Fig. 8). The FT-IR spectrum of the catalyst after use (Fig. 8b) showed no significant changes than the specrum of the catalyst before use (Fig. 8a). This reveals that the catalyst is durable, and remains constant during the reaction. Therefore, it can reuse in further runs without significant loss in its activity and is capable to catalyze the reaction after each run successfully.

2.3. Investigation of reaction mechanism

A proposed mechanism for the BPPT NPs catalyzed the synthesis of 4*H*-chromene derivatives has shown in Scheme 3. As can be seen from the mechanism, 4*H*-chromene **8** is obtained through a multi-step route including Knoevenagel condensation, Michael addition reaction and intramolecular cyclization from reaction between methyl cyanoacetate **5**, aryl aldehyde **6** and dimedone **7** in the presence of catalytic amount of BPPT NPs. By a closer look at Scheme 3, it is revealed that in all steps BPPT NPs act as activator and accelerate reaction progress via its Brønsted base virtue. In first step, BPPT NPs activate methyl cyanoacetate **5** for nucleophilic attack to aldehyde **6** and leads to formation of int. **9**. Next, dehydration of int. **9** in the presence of BPPT NPs gives Knoevenagel intermediate **10**. On the other hand, BPPT NPs activate dimedone **7** to nucleophilic attack to Knoevenagel intermediate **10** (Michael addition reaction). By this reaction, int. **11** is formed. Subsequent intramolecular cyclization of int. **11** in the presence of BPPT NPs gives int. **12**. In the final step, product **8** is obtained by imine-enamine tautomerization of int. **12**.

2.4. Molecular docking studies

The containing of alkylamine side chain in BPPT chemical structure and considering the structures of drugs that inhibit acetylcholinesterase enzyme such as donepezil, and rivastigmine (used for the treatment of Alzheimer, Parkinson, and Autism), and also other potent acetylcholinesterase inhibitors that have contained piperidine or piperazine side chains in their structures (Liu et al., 2018a; Mohamed et al., 2018), we decided to study molecular docking for BPPT, and compare the results

Table 3
Synthesis of 4*H*-chromene derivatives using BPPT NPs.[a]

Compound[b]	Ar	Time (min)/ (lit.)	Yield[c] (%)/(lit.)	M.P. (lit.)
8a	4-(2-morpholinoethoxy)-C_6H_4	60	87	174–175[d]
8b	4-(4-morpholino)-C_6H_4	60	85	188–189[d]
8c	4-(4-piperidin-1-yl)-C_6H_4	60	80	170–173[d]
8d	4-(4-chlorobenzyloxy)-C_6H_4	40	95	158–160[d]
8e	3-(4-chlorobenzyloxy)-C_6H_4	45	92	159–161[d]
8f	4-(4-bromobenzyloxy)-C_6H_4	40	95	158–161[d]
8g	3-(4-bromobenzyloxy)-C_6H_4	50	93	164–167[d]
8h	4-F-C_6H_4	40	90	143–145[d]
8i	3-Br-C_6H_4	45	88	174–176[d]
8j	2-Br-C_6H_4	45	91	197–200[d]
8k	C_6H_5	40/10	88/92	145-147 (144–146) (Rong et al., 2006)
8l	4-Cl-C_6H_4	40/20	91/91	167-169 (170–171) (Guo et al., 2013)
8m	2-Cl-C_6H_4	40/60	91/70	196-199 (198–200) (Wang et al., 2003)
8n	3-Cl-C_6H_4	40/60	87/86	178-179 (178–179) (Li et al., 2006)
8°	4-NO_2-C_6H_4	30/18	94/92	181-183 (187–188) (Guo et al., 2013)
8p	3-NO_2-C_6H_4	30/20	93/80	190-192 (191–192) (Patra and Mahapatra, 2010)
8q	2-NO_2-C_6H_4	30/60	95/87	187-189 (188–189) (Li et al., 2006)
8r	4-CH_3-C_6H_4	40/10	91/90	178-181 (172) (Rong et al., 2006)

[a] Reaction conditions: methyl cyanoacetate (1.25 mmol), aryl aldehyde (1 mmol), dimedone (1 mmol), nanocatalyst (5 mol%), EtOH (8 mL), 70 °C.
[b] The chemical structures of compounds are listed in Fig. 6.
[c] Refers to isolated yields.
[d] Novel compounds.

with the Donepezil as reference drug to treatment of Alzheimer (Fig. 9). As can be seen from Fig. 9a, BPPT interacted with donepezil binding site of AChE as great as donepezil. Also in Fig. 9b, it is clearer that BPPT has an excellent matching in width and length with donepezil and exactly overlap with donepezil structure to interact with AChE enzyme.

The investigation of molecular interaction of BPPT with AChE revealed that there are five significant interactions that are two π-cation interactions between NH_2^+ groups with TRP86 and TRP286, two H-bond interactions between oxygen with TYR124, and GLU202 with NH_2^+ group, and finally a salt-bridge interaction between NH_2^+ group with GLU202 (Fig. 10).

In addition, docking results indicated Glide XP G-score (a parameter corresponding ligand-protein stability in which more negative scores are related to better fillers and imply less steric hindrance and signifies that the ligand can fill the poses of the protein very well) of BPPT (-10.323) is close to donepezil (-16.144) (Table 4).

Therefore, docking studies represented that BPPT has a great affinity with donepezil structure to bind and block the sites of the AChE enzyme.

2.5. ADMETox prediction

In another supplement survey, to investigate the biological properties of BPPT and the prediction that can it be a good candidate as AChE inhibitor?, *In silico* ADMETox prediction study was performed, compared with donepezil, and the results were summarized in Table 4. ADMETox prediction revealed that BPPT has no variation from Lipinski's rule of five as of donepezil. It can permeate into the blood-brain barrier (BBB) as good as donepezil. Both BPPT and donepezil are capable of binding well to human serum albumin, but their quantitative human oral absorptions are not identical. As predicted results showed, quantitative human oral absorptions of BPPT is not as good as donepezil. As well as, predicted IC_{50} for the blockage of HERG K^+ channels in heart for both BPPT and donepezil was not in acceptable range, therefore they could be the HERG K^+ channels blockers. On the other hand, HERG K^+ channels blocking of donepezil has previously been proved and considered as one of the known side-effects of the Donepezil. It can induce "torsades de point" which is characterized as marked QT prolongation in electrocardiogram, and may result in cardiac syncope (Kitt et al., 2015). This side-effect is known to be related to the inhibition of hERG protein in cardiomyocytes (Kitt et al., 2015). This fact can further confirm the accuracy of our prediction tool. Overall, ADMETox prediction depicted that BPPT can be a good candidate for AChE inhibitors and can be a lead compound for further discoveries of anti-Alzheimer drugs.

3. Experimental

All used chemicals were supplied from Merck or Sigma-Aldrich as mercantile chemical companies. An Electrothermal-9100 apparatus was applied to record melting points and all of them are uncorrected. Elemental analyses of compounds were carried out by a Heracus CHN-O-Rapid analyzer. An FT-IR Magna 550 spectrophotometer (Nicolet) using KBr as a carrier was applied to record FT-IR spectra. All FT-NMRs were taken by an FT-NMR Bruker 300 MHz spectrometer. The progress of the reactions was monitored by thin-layer chromatography (Silica TLC F_{254} plates, eluent: ethyl acetate/*n*-hexane v/v = 1:1). Scanning electron microscopy (SEM) evaluations of the nano-catalyst were performed on a JEOL JEM 3010 instrument operating at an accelerating voltage of 300 kV. Transmission electron microscopy (TEM) investigations of the nano-catalyst were performed on a JEOL JEM 3010 instrument operating at an accelerating voltage of 300 kV. Thermogravimetric (TG) measurements were carried out using a thermal gravimetric analyzer (BAHR, STA 503) from room temperature to 1100 °C in air at a heating rate of 10 °C min^{-1}. Acetylcholinesterase (AChE) structure was extracted from the Protein Data Bank (PDB) database which was co-crystalized with Donepezil as an antagonist. The protein structure was prepared in pH = 7.4 ± 1 using the Maestro interface of Schrodinger Suite. Het groups and waters with less than 3 hydrogen bonds to non-waters were removed and hydrogen bonds were reassigned using PROPKA. A final minimization of the structure to an RMSD of less than 0.3 Å was performed to remove atom clashes and reduce steric hindrance. The binding site of Donepezil with AChE was used as a pattern to create grid-files for computational molecular docking.

The structure of BPPT was drawn in Chemdraw software and optimized using Ligprep with Optimized Potential for Liquid Simulations 3 (OPLS3) force-field and the 3D-optimized form was generated in pH = 7.4 ± 1. Computational molecular docking was performed using Glide module with extra precision (XP) method (Friesner et al., 2006) for both BPPT and Donepezil as a reference compound. Ligand sampling was set to flexible (including ring conformations and nitrogen inversions and Epik state penalties were incorporated to docking scores. A post docking minimization was applied by employing strain correction terms. Maestro

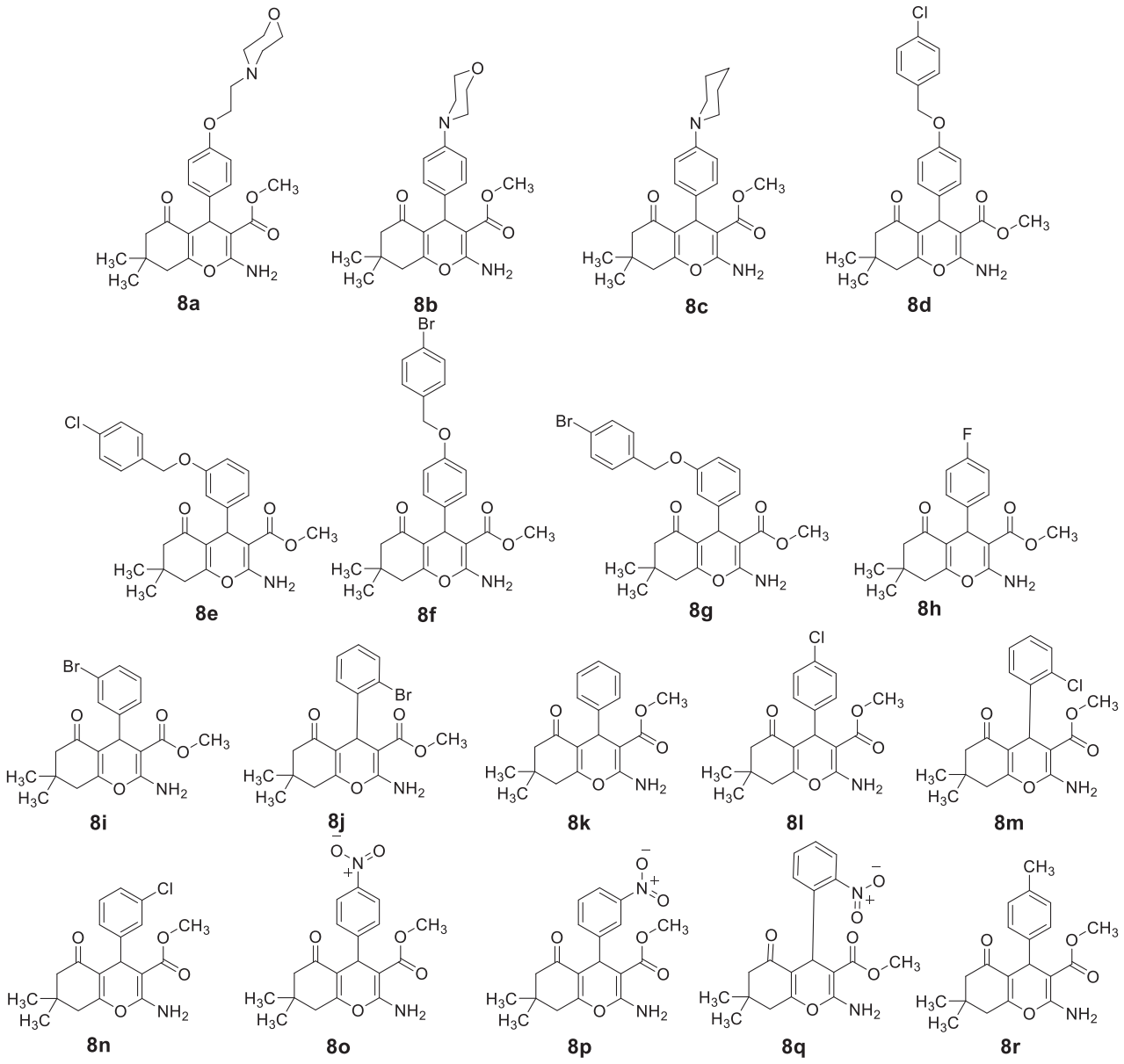

Fig. 6. The chemical structures of synthesized compounds.

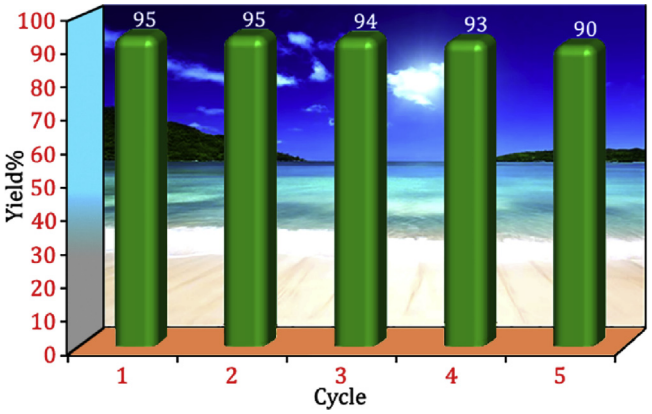

Fig. 7. Recyclability studies of BPPT NPs on model reaction.

interface was used as the molecular visualization of all figures.

Absorption, Distribution, Metabolism, Excretion, and Toxicity of the BPPT, was assessed using QikProp. Blood-Brain Barrier (BBB) permeability, percent of human oral absorption, prediction of binding to human serum albumin and IC_{50} for the blockage of HERG K^+ channels in heart, and also ligand-protein stability score for BPPT were compared with donepezil as a reference drug.

3.1. *Preparation of BPPT NPs*

Sodium tungstate dihydrate (7 g) was firstly dried by a vacuum oven under 120 °C for 6 h. Next, anhydrous sodium tungstate **1** (20 mmol, 5.88 g) was gradually added to a stirred 250 mL round bottom flask containing 1-bromo-3-chloropropane **2** (40 mmol, 6.28 g) in 50 mL *n*-hexane at room temperature during 15 min. After 48 h, the reaction mixture was filtrate to separate bis(3-chloropropyl)tungstate **3**. Obtained solid material **3** was washed with distilled water to remove side product, sodium bromide salt. 15 mL distilled water in five times (3 mL in each time) was used until filtrate become free of bromide ion. To identification of bromide ion silver

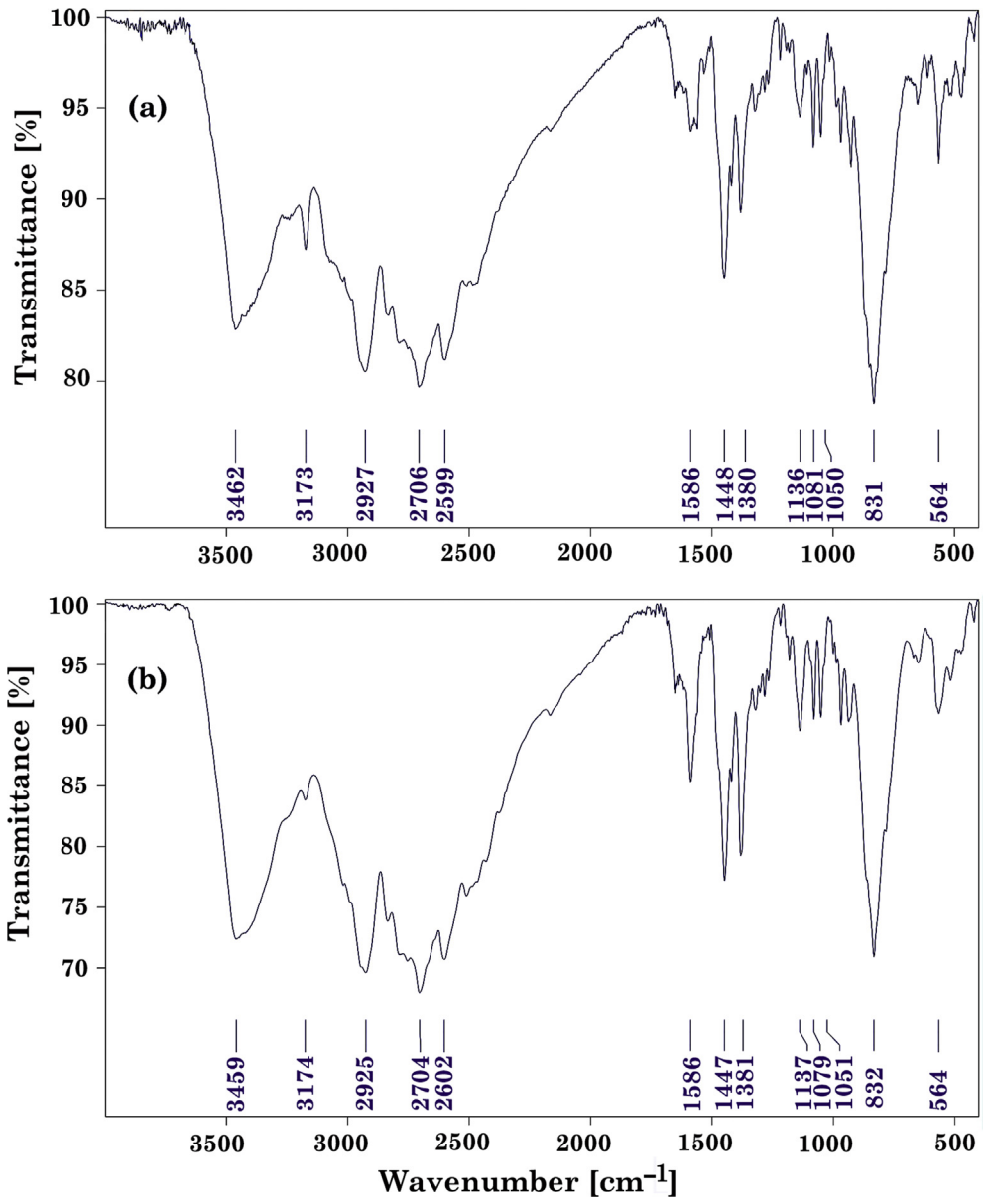

Fig. 8. The FT-IR spectra of the catalyst (a) befor and (b) after use.

nitrate solution (0.05 M) was applied. Solid material **3** was dried in vacuum oven at 100 °C for 5 h. In the next step, to a 250 mL round bottom flask containing 60 mL toluene equipped with reflux condenser, connected to a water bowl by a hoses interface, solid **3** (16 mmol, 6.4 g) was added, then piperazine **4** (32 mmol, 2.8 g) was gradually added to the flask during 15 min. When the addition of piperazine was completed, it was allowed to the reaction mixture to stir for 0.5 h in room temperature and then 48 h under reflux conditions. Afterward, the reaction mixture was filtrated to obtain BPPT. Finally, after drying catalyst at 100 °C for 5 h, 28 g BPPT was obtained and was characterized by FT-IR spectroscopy, TEM, and SEM microscopes and also TGA measurement.

3.2. General procedure to the synthesis of methyl 2-amino-7,7-dimethyl-5-oxo-4-aryl substituted-5,6,7,8-tetrahydro-4H-chromene-3-carboxylate

To a stirred round bottom flask containing ethanol (12 mL) along with catalytically amounts of BPPT (0.50 g, 5 mol%), appropriate aryl aldehyde (2.0 mmol), and methyl cyanoacetate (2.5 mmol, 0.25 g) was added. After stirring reaction mixture for 1 h at room temperature, dimedone (2.0 mmol, 0.280 g) was added, and it was allowed to the mixture's temperature to rise at 70 °C. The reaction progress was monitored by TLC (ethyl acetate/*n*-hexane v/v = 1:1). After passing the appropriate time, indicated in Table 2, the boiling ethanol (50 mL) was added to the reaction mixture till crude products completely dissolved, then the mixture was filtered to separate catalyst. The catalyst was washed with boiling ethanol, dried at 100 °C for 2 h and reused in another cycle. The filtrate was evaporated to obtain the crude product. The crystalline pure product was obtained from the crystallization of crude product in boiling ethanol. The chemical structures of novel crystalline pure products were confirmed by FT-IR, ^{1}H NMR, ^{13}C NMR spectroscopies, elemental analyses (C, H, N) and for known compounds via comparison of their melting points with the reported ones.

3.3. Spectroscopic data of novel synthesized products

Methyl 2-amino-7,7-dimethyl-4-(4-(2-morpholinoethoxy)phenyl)-5-oxo-5,6,7,8-tetrahydro-4*H*-chromene-3-carboxylate **(8a):** Snow white powder, m.p: 174–175 °C; FT-IR (KBr) ($\bar{\upsilon}_{max}$, cm^{-1}): 3387, 3284, 3060,

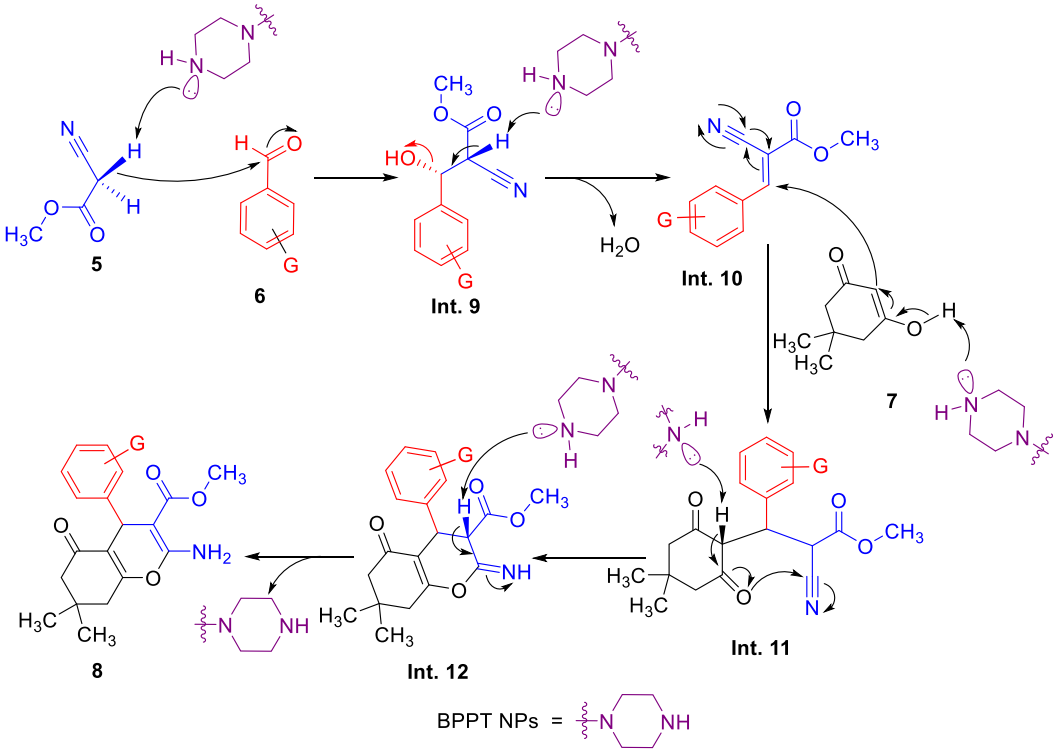

Scheme 3. Proposed mechanism for the BPPT NPs-catalyzed synthesis of 4*H*-chromene derivatives.

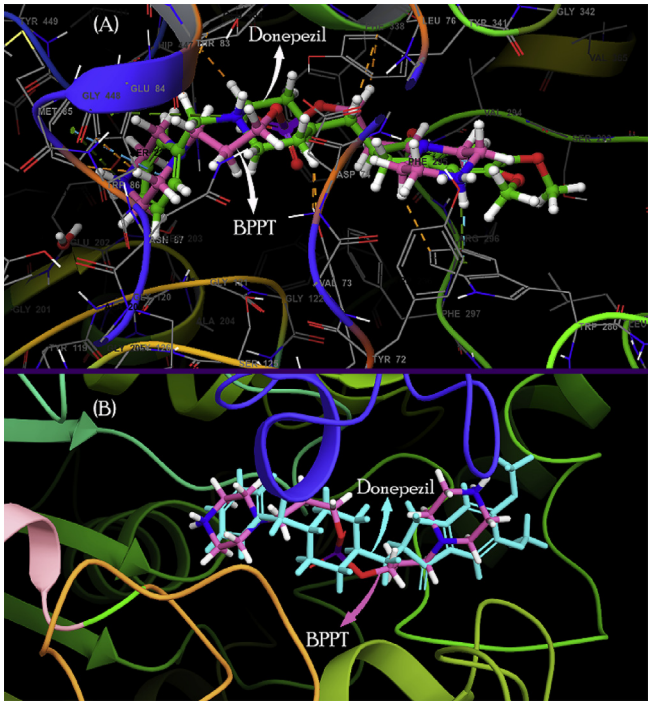

Fig. 9. (a) Molecular interactions of BPPT and Donepezil (reference drug) with AChE enzyme. (b) The great structural matching of BPPT with donepezil to interact with AChE enzyme.

2958, 2865, 2801, 1693, 1693, 1669, 1534, 1509, 1365, 1295, 1251, 1201, 1146, 1037, 846, 541. ^{1}H NMR (DMSO-d_6, 300 MHz) δ (ppm): 7.55 (2H, s, NH_2), 7.04 (2H, d, J = 9 Hz, CH_{Ar}), 6.78 (2H, d, J = 9 Hz, CH_{Ar}), 4.47 (1H, s, CH), 4.02 (2H, t, J = 6 Hz, OCH_2), 3.59 (4H, t, J = 6 Hz, CH_2OCH_2), 3.52 (3H, s, OCH_3), 2.69 (2H, t, J = 6 Hz, NCH_2), 2.52 (4H, t, J = 6 Hz, CH_2NCH_2), 2.49 (2H, m, CH_2), 2.27 (1H, d, J = 15 Hz, CH), 2.06 (1H, d, J = 15 Hz, CH), 1.05 (3H, s, CH_3), 0.90 (3H, s, CH_3). ^{13}C NMR (DMSO-d_6, 75 MHz) δ (ppm): 196.3, 168.8, 162.3, 159.7, 157.0, 138.9, 128.8, 116.3, 114.2, 78.3, 66.5, 65.4, 57.5, 54.0, 50.9, 50.4, 32.6, 32.3, 29.1, 26.9. Anal. calcd for $C_{25}H_{32}N_2O_6$: C, 65.77; H, 7.07; N, 6.14; Found: C, 65.81; H, 7.12; N, 6.09%.

Methyl 2-amino-7,7-dimethyl-4-(4-morpholinophenyl)-5-oxo-5,6,7,8-tetrahydro-4*H*-chrome-ne-3-carboxylate **(8b):** Light yellow crystals, m.p: 188–189 °C; FT-IR (KBr) ($\bar{u}_{max}$, cm^{-1}): 3390, 3280, 3058, 2957, 2870, 2822, 1690, 1652, 1609, 1529, 1439, 1364, 1287, 1156, 1120, 1104, 921. ^{1}H NMR (DMSO-d_6, 300 MHz) δ (ppm): 7.52 (2H, s, NH_2), 6.99 (2H, d, J = 9Hz, CH_{Ar}), 6.79 (2H, d, J = 9 Hz, CH_{Ar}), 4.44 (1H, s, CH), 3.71 (4H, brs, CH_2OCH_2), 3.36 (3H, s, OCH_3), 3.04 (4H, brs, CH_2NCH_2), 2.52 (2H, m, CH_2), 2.27 (1H, d, J = 15 Hz, CH), 2.07 (1H, d, J = 15 Hz, CH), 1.05 (3H, s, CH_3), 0.91 (3H, s, CH_3). ^{13}C NMR (DMSO-d_6, 75 MHz) δ (ppm): 196.3, 168.9, 162.3, 159.7, 149.5, 137.6, 128.4, 116.4, 115.1, 78.5, 66.6, 50.9, 50.5, 49.0, 32.5, 32.3, 29.1, 27.0. Anal. calcd for $C_{23}H_{28}N_2O_5$: C, 66.97; H, 6.84; N, 6.79; Found: C, 67.05; H, 6.79; N, 6.83%.

Methyl 2-amino-7,7-dimethyl-5-oxo-4-(4-(piperidin-1-yl)phenyl)-5,6,7,8-tetrahydro-4*H*-chr-omene-3-carboxylate **(8c):** Golden rod crystals, m.p: 170–173 °C; FT-IR (KBr) ($\bar{u}_{max}$, cm^{-1}): 3412, 3301, 3085, 2933, 2853, 2792, 1695, 1656, 1612, 1513, 1437, 1367, 1288, 1204, 1164, 1036, 840, 497. ^{1}H NMR (DMSO-d_6, 300 MHz) δ (ppm): 7.52 (2H, s, NH_2), 6.98 (2H, d, J = 9 Hz, CH_{Ar}), 6.77 (2H, d, J = 9 Hz, CH_{Ar}), 4.44 (1H, s, CH), 3.53 (3H, s, OCH_3), 3.04 (4H, t, J = 6 Hz, CH_2NCH_2), 2.54 (1H, d, J = 18 Hz, CH), 2.54 (1H, d, J = 18 Hz, CH), 2.27 (1H, d, J = 15 Hz, CH), 2.08 (1H, d, J = 15 Hz, CH), 1.59 (4H, m, 2×CH_2), 1.51 (2H, m, CH_2), 1.05 (3H, s, CH_3), 0.92 (3H, s, CH_3). ^{13}C NMR (DMSO-d_6, 75 MHz) δ (ppm): 196.3, 168.9, 162.2, 159.7, 150.3, 136.9, 128.3, 116.5, 115.8, 78.5, 50.9, 50.5, 50.1, 32.4, 32.3, 29.1, 26.9, 25.9, 24.3. Anal. calcd for C24H30N2O4: C, 70.22; H, 7.37; N, 6.82; Found: C, 70.27; H, 7.31; N, 6.85%.

Methyl 2-amino-4-(4-((4-chlorobenzyl)oxy)phenyl)-7,7-dimethyl-5-oxo-5,6,7,8-tetrahydro-4H-chromene-3-carboxylate **(8d):** White crystals, m.p: 158–160 °C; FT-IR (KBr) ($\bar{u}_{max}$, cm^{-1}): 3431, 3315, 3060, 2953,

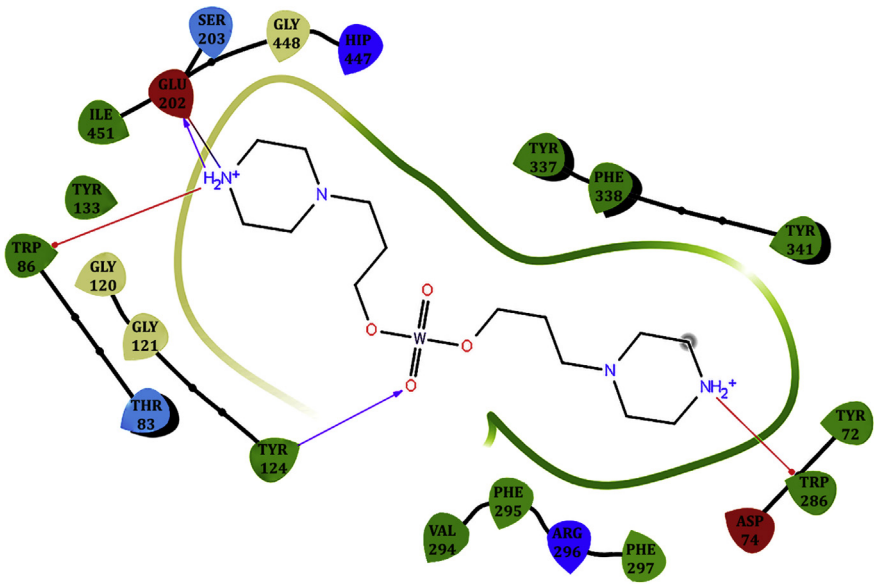

Fig. 10. The most significant interactions between BPPT and AChE enzyme.

Table 4
In silico prediction of pharmacokinetic/pharmacodynamic characteristics of BPPT to inhibition of AChE versus Donepezil.

Compound	Rule of Five	QplogBB[a]	QPlogKhsa[b]	Human Oral Absorption[c]	QPlogHERG[d]	XP G-score[e]
Donepezil[f]	0	0.063	0.597	100 %	-6.528	-16.144
BPPT	0	-0.526	-0.741	37.9 %	-7.405	-10.323

[a] Predicted blood-brain barrier coefficient (Recommended Range: -3 – 1.2).
[b] Prediction of binding to human serum albumin (Recommended. Range: -1.5 – 1.5).
[c] Predicted quantitative human oral absorption on 0–100% scale; >80% is high and <25% is poor.
[d] Predicted IC_{50} for the blockage of HERG K^+ channels in the heart (concern below -5).
[e] A parameter corresponding ligand-protein stability that more negatives values imply that the poses of the target protein (binding sites) are filled by the ligand very good.
[f] Reference drug.

2929, 2869, 1688, 1666, 1606, 1506, 1368, 1300, 1233, 1200, 1163, 1014, 875, 814, 559, 539. ^{1}H NMR (DMSO-d_6, 300 MHz) δ (ppm): 7.56 (2H, s, NH_2), 7.46 (4H, m, CH_{Ar}), 7.07 (2H, d, $J = 6$ Hz, CH_{Ar}), 6.86 (2H, d, $J = 6$ Hz, CH_{Ar}), 5.03 (2H, s, OCH_2), 4.49 (1H, s, CH), 3.52 (3H, s, OCH_3), 2.55 (1H, d, $J = 18$ Hz, CH), 2.46 (1H, d, $J = 18$ Hz, CH), 2.27 (1H, d, $J = 15$ Hz, CH), 2.07 (1H, d, $J = 15$ Hz, CH), 1.05 (3H, s, CH_3), 0.90 (3H, s, CH_3). ^{13}C NMR (DMSO-d_6, 75 MHz) δ (ppm): 196.2, 168.8, 162.4, 159.7, 156.8, 139.3, 136.7, 132.8, 129.9, 128.9, 128.8, 116.3, 114.5, 78.3, 68.7, 50.9, 50.4, 32.7, 32.3, 29.1, 26.9. Anal. calcd for $C_{26}H_{26}ClNO_5$: C, 66.74; H, 5.60; N, 2.99; Found: C, 66.80; H, 5.55; N, 3.07%.

Methyl 2-amino-4-(3-((4-chlorobenzyl)oxy)phenyl)-7,7-dimethyl-5-oxo-5,6,7,8-tetrahydro-4H-chromene-3-carboxylate (**8e**): Snow white crystals, m.p: 159–161 °C; FT-IR (KBr) ($\bar{\upsilon}_{max}$, cm^{-1}): 3416, 3302, 3064, 2950, 2868, 1691, 1655, 1612, 1517, 1439, 1370, 1291, 1249, 1202, 1171, 1028, 802, 689, 491. ^{1}H NMR (DMSO-d_6, 300 MHz) δ (ppm): 7.60 (2H, s, NH_2), 7.47 (4H, m, CH_{Ar}), 7.14 (1H, t, $J = 9$ Hz, CH_{Ar}), 6.79–6.76 (2H, m, CH_{Ar}), 6.74 (1H, s, CH_{Ar}), 5.05 (2H, dd, $^3J = 15$ Hz, $^4J = 6$ Hz, OCH_2), 4.52 (1H, s, CH), 3.52 (3H, s, OCH_3), 2.55 (1H, d, $J = 18$ Hz, CH), 2.45 (1H, d, $J = 18$ Hz, CH), 2.27 (1H, d, $J = 15$ Hz, CH), 2.07 (1H, d, $J = 18$ Hz, CH), 1.04 (3H, s, CH_3), 0.89 (3H,s,CH_3). ^{13}C NMR (DMSO-d_6, 75 MHz) δ (ppm): 196.2, 168.7, 162.7, 159.8, 158.2, 148.4, 136.6, 132.8, 129.9, 129.3, 128.9, 120.5, 116.0, 114.8, 112.2, 77.8, 68.7, 50.9, 50.4, 33.4, 32.3, 29.0, 26.9. Anal. calcd for $C_{26}H_{26}ClNO_5$: C, 66.74; H, 5.60; N, 2.99; Found: C, 66.79; H, 5.63; N, 3.05%.

Methyl 2-amino-4-(4-((4-bromobenzyl)oxy)phenyl)-7,7-dimethyl-5-oxo-5,6,7,8-tetrahydro-4H-chromene-3-carboxylate (**8f**): Snow white crystals, m.p: 158–161 °C; FT-IR (KBr) ($\bar{\upsilon}_{max}$, cm^{-1}): 3434, 3315, 3049, 2954, 2926, 1688, 1666, 1606, 1506, 1436, 1369, 1300, 1234, 1199, 1163, 1012, 873, 810, 555. ^{1}H NMR (DMSO-d_6, 300 MHz) δ (ppm): 7.61 (2H, s, NH_2), 7.57 (2H, d, $J = 6$ Hz, CH_{Ar}), 7.40 (2H, d, $J = 6$ Hz, CH_{Ar}), 7.06 (2H, d, $J = 9$ Hz, CH_{Ar}), 6.86 (2H, d, $J = 9$ Hz, CH_{Ar}), 5.01 (2H, s, OCH_2), 4.48 (1H, s, CH), 3.52 (3H, s, OCH_3), 2.55 (1H, d, $J = 15$ Hz, CH), 2.45 (1H, d, $J = 15$ Hz, CH), 2.27 (1H, d, $J = 15$ Hz, CH), 2.07 (1H, d, $J = 15$ Hz, CH), 1.05 (3H, s, CH_3), 0.90 (3H,s,CH_3). ^{13}C NMR (DMSO-d_6, 75 MHz) δ (ppm): 196.3, 168.8, 162.4, 159.7, 156.8, 139.3, 137.1, 131.8, 130.2, 128.9, 121.3, 116.3, 114.5, 78.2, 68.7, 51.0, 50.4, 32.6, 32.3, 29.1, 26.9. Anal. calcd for $C_{26}H_{26}BrNO_5$: C, 60.95; H, 5.11; N, 2.73; Found: C, 60.99; H, 5.06; N, 2.80%.

Methyl 2-amino-4-(3-((4-bromobenzyl)oxy)phenyl)-7,7-dimethyl-5-oxo-5,6,7,8-tetrahydro-4H-chromene-3-carboxylate (**8g**): Snow white crystals, m.p: 164–167 °C; FT-IR (KBr) ($\bar{\upsilon}_{max}$, cm^{-1}): 3415, 3300, 3050, 2948, 2867, 1690, 1655, 1595, 1517, 1439, 1370, 1290, 1249, 1202, 1172, 1027, 802, 778, 689, 495. ^{1}H NMR (DMSO-d_6, 300 MHz) δ (ppm): 7.60 (2H, d, $J = 9$ Hz, CH_{Ar}), 7.58 (2H, s, NH_2), 7.41 (2H, d, $J = 9$ Hz, CH_{Ar}), 7.14 (1H, t, $J = 9$ Hz, CH_{Ar}), 6.79–6.75 (2H, m, CH_{Ar}), 6.74 (1H, s, CH_{Ar}), 5.03 (2H, dd, $^3J = 18$ Hz, $^4J = 6$ Hz, OCH_2), 4.52 (1H, s, CH), 3.51 (3H, s, OCH_3), 2.55 (1H, d, $J = 18$ Hz, CH), 2.45 (1H, d, $J = 18$ Hz, CH), 2.27 (1H, d, $J = 15$ Hz, CH), 2.06 (1H, d, $J = 15$ Hz, CH), 1.04 (3H, s, CH_3), 0.88 (3H, s, CH_3). ^{13}C NMR (DMSO-d_6, 75 MHz) δ (ppm): 196.2, 168.7, 162.7, 159.8, 158.2, 148.3, 137.1, 131.8, 130.2, 129.3, 121.3, 120.5, 116.0, 114.8, 112.3, 77.8, 68.7, 51.0, 50.4, 33.4, 32.3, 29.0, 26.9. Anal. calcd for $C_{26}H_{26}BrNO_5$: C, 60.95; H, 5.11; N, 2.73; Found: C, 61.01; H, 5.05; N, 2.81%.

Methyl 2-amino-4-(4-fluorophenyl)-7,7-dimethyl-5-oxo-5,6,7,8-tetrahydro-4H-chromene-3-carboxylate (**8h**): White powder, m.p:

143–145 °C; FT-IR (KBr) ($\bar{\upsilon}_{max}$, cm^{-1}): 3464, 3309, 3040, 2967, 2935, 1694, 1657, 1526, 1506, 1436, 1365, 1295, 1224, 1198, 1163, 1036, 849, 769, 645, 542. ^{1}H NMR (DMSO-d_6, 300 MHz) δ (ppm): 7.37 (2H, s, NH_2), 6.91 (2H, d, $J = 9$ Hz, CH_{Ar}), 6.79 (2H, t, $J = 9$ Hz, CH_{Ar}), 4.28 (1H, s, CH), 3.27 (3H, s, OCH_3), 2.31 (1H, d, $J = 18$ Hz, CH), 2.22 (1H, d, $J = 18$ Hz, CH), 2.03 (1H, d, $J = 15$ Hz, CH), 1.83 (1H, d, $J = 15$ Hz, CH), 0.80 (3H, s, CH_3), 0.65 (3H, s, CH_3). ^{13}C NMR (DMSO-d_6, 75 MHz) δ (ppm): 196.2, 168.7, 162.6, 159.7, 142.9, 129.7 (d, $J = 7.5$ Hz), 115.9, 115.1, 114.8, 77.8, 51.0, 50.3, 33.0, 32.3, 29.0, 26.9. Anal. calcd for $C_{19}H_{20}FNO_4$: C, 66.08; H, 5.84; N, 4.06; Found: C, 66.13; H, 5.78; N, 4.10%.

Methyl 2-amino-4-(3-bromophenyl)-7,7-dimethyl-5-oxo-5,6,7,8-tetrahydro-4H-chromene-3-carboxylate (**8i**): White crystals, m.p: 174–176 °C; FT-IR (KBr) ($\bar{\upsilon}_{max}$, cm^{-1}): 3399, 3298, 3043, 2960, 2875, 1696, 1656, 1535, 1437, 1365, 1286, 1200, 1163, 1072, 1034, 771, 695, 514. ^{1}H NMR (DMSO-d_6, 300 MHz) δ (ppm): 7.66 (2H, s, NH_2), 7.33–7.30 (1H, m, CH_{Ar}), 7.28 (1H, s, CH_{Ar}), 7.21 (1H, t, $J = 9$ Hz, CH_{Ar}), 7.17–7.14 (1H, m, CH_{Ar}), 4.51 (1H, s, CH), 3.53 (3H, s, OCH_3), 2.57 (1H, d, $J = 15$ Hz, CH), 2.50 (1H, d, $J = 15$ Hz, CH), 2.30 (1H, d, $J = 15$ Hz, CH), 2.10 (1H, d, $J = 15$ Hz, CH), 1.05 (3H, s, CH_3), 0.90 (3H, s, CH_3). ^{13}C NMR (DMSO-d_6, 75 MHz) δ (ppm): 196.3, 168.5, 163.0, 159.7, 149.5, 130.7, 130.6, 129.2, 127.1, 121.5, 115.4, 77.3, 51.0, 50.3, 33.6, 32.3, 29.0, 26.8. Anal. calcd for $C_{19}H_{20}BrNO_4$: C, 56.17; H, 4.96; N, 3.45; Found: C, 56.10; H, 4.88; N, 3.51%.

Methyl 2-amino-4-(2-bromophenyl)-7,7-dimethyl-5-oxo-5,6,7,8-tetrahydro-4H-chromene-3-carboxylate (**8j**): White crystals, m.p: 197–200 °C; FT-IR (KBr) ($\bar{\upsilon}_{max}$, cm^{-1}): 3424, 3313, 3045, 2966, 2924, 1693, 1651, 1610, 1516, 1437, 1362, 1289, 1202, 1082, 1037, 828, 761, 739, 506. ^{1}H NMR (DMSO-d_6, 300 MHz) δ (ppm): 7.67 (2H, s, NH_2), 7.45 (1H, dd, $^3J = 9$ Hz, $^4J = 3$ Hz, CH_{Ar}), 7.25 (1H, dt, $^3J = 9$ Hz, $^4J = 3$ Hz, CH_{Ar}), 7.16 (1H, dd, $^3J = 9$ Hz, $^4J = 3$ Hz, CH_{Ar}), 7.02 (1H, dt, $^3J = 9$ Hz, $^4J = 3$ Hz, CH_{Ar}), 4.86 (1H, s, CH), 3.47 (3H, s, OCH_3), 2.59 (1H, d, $J = 18$ Hz, CH), 2.44 (1H, d, $J = 18$ Hz, CH), 2.26 (1H, d, $J = 15$ Hz, CH), 2.02 (1H, d, $J = 15$ Hz, CH), 1.05 (3H, s, CH_3), 0.91 (3H, s, CH_3). ^{13}C NMR (DMSO-d_6, 75 MHz) δ (ppm): 196.0, 168.9, 162.6, 159.6, 145.3, 133.0, 131.7, 128.0, 127.7, 123.7, 115.0, 77.2, 50.7, 50.5, 34.3, 32.2, 29.1, 26.9. Anal. calcd for $C_{19}H_{20}BrNO_4$: C, 56.17; H, 4.96; N, 3.45; Found: C, 56.23; H, 4.89; N, 3.49%.

4. Conclusions

In conclusion, we found BPPT NPs as an efficient, and eco-friendly heterogeneous recyclable organometallic Brønsted base which can catalyze successfully multi-step reaction including Knoevenagel condensation, Michael addition reaction and intramolecular cyclization between methyl cyanoacetate, aryl aldehydes, and dimedone to yield 4*H*-chromene derivatives in good to excellent yields. Therefore, BPPT NPs can be applied as a catalyst in reactions in which needs basic catalyst or media. Hence, it can attract many interests and find many applications in organic syntheses in future. This methodology not only produces the products with excellent yields in short reaction times but also keeps away from some disadvantages such as catalyst handling and cost, pollution and safety. Also, easy work-up, recyclability and thermal stability of catalyst are other advantages of BPPT NPs. In addition, molecular modeling and ADMETox prediction results showed that BPPT can be considered as a potent AChE inhibitor, and can be a lead compound to further discovery of anti-Alzheimer drugs.

Declarations

Author contribution statement

Khalil Eskandari: Conceived and designed the experiments; Performed the experiments; Analyzed and interpreted the data; Contributed reagents, materials, analysis tools or data; Wrote the paper.

Yaghoub Pourshojaei: Conceived and designed the experiments; Analyzed and interpreted the data; Contributed reagents, materials, analysis tools or data; Wrote the paper.

Fatemeh Haghani, Mahnaz Shabani: Performed the experiments.

Ali Asadipour: Conceived and designed the experiments; Analyzed and interpreted the data; Contributed reagents, materials, analysis tools or data.

Funding statement

This work was supported by the Pharmaceutics Research Center, Institute of Neuropharmacology, Kerman University of Medical Sciences.

Competing interest statement

The authors declare no conflict of interest.

Additional information

Supplementary content related to this article has been published online at https://doi.org/10.1016/j.heliyon.2019.e02426.

Acknowledgements

The authors are thankful to all their colleagues for their assistance and encouragement especially to Prof. Bahador Karami, Prof. Abbas Pardakhty, Prof. Alireza Foroumadi, and Dr. Hojjat Samareh-Fekri who sporadically offered their experience and knowledge.

References

Alinezhad, H., Tarahomi, M., Maleki, B., Amiri, A., 2019. SO_3 H-functionalized nano-MGO-D-NH_2: synthesis, characterization and application for one-pot synthesis of pyrano[2,3-d] pyrimidinone and tetrahydrobenzo[b]pyran derivatives in aqueous media. Appl. Organomet. Chem. 33 e4661.

Alzeer, M.I.M., MacKenzie, K.J.D., 2018. Synthesis and catalytic properties of new sustainable aluminosilicate heterogeneous catalysts derived from fly ash. ACS Sustain. Chem. Eng. 6, 5273–5282.

Antonangelo, A.R., Westrup, K.C.M., Burt, L.A., Bezzu, C.G., Malewschik, T., Machado, G.S., Nunes, F.S., McKeown, N.B., Nakagaki, S., 2017. Synthesis, crystallographic characterization and homogeneous catalytic activity of novel unsymmetric porphyrins. RSC Adv. 7, 50610–50618.

Asadipour, A., Pourshojaei, Y., Eskandari, K., Foroumadi, A., 2017. A short synthesis of 7-amino alkoxy homoisoflavonoides. RSC Adv. 7, 44680–44687.

Asadipour, A., Shams, Z., Eskandari, K., Moshafi, M.H., Faghih-Mirzaei, E., Pourshojaei, Y., 2018. Efficient, straightforward, catalyst-free synthesis of medicinally important S-alkyl/benzyl dithiocarbamates under green conditions. Res. Chem. Intermed. 44, 1295–1304.

Aune, D., Keum, N., Giovannucci, E., Fadnes, L.T., Boffetta, P., Greenwood, D.C., Tonstad, S., Vatten, L.J., Riboli, E., Norat, T., 2018. Dietary intake and blood concentrations of antioxidants and the risk of cardiovascular disease, total cancer, and all-cause mortality: a systematic review and dose-response meta-analysis of prospective studies. Am. J. Clin. Nutr.

Banoth, S., Boda, S., Perugu, S., Balabadra, S., Manga, V., 2018. Design, synthesis, biological evaluation and in silico molecular docking studies of novel benzochromeno[2,3-d]thiazolopyrimidine derivatives. Res. Chem. Intermed. 44, 1833–1846.

Brückner, A., Bentrup, U., Zanthoff, H., Maschmeyer, D., 2009. The role of different Ni sites in supported nickel catalysts for butene dimerization under industry-like conditions. J. Catal. 266, 120–128.

Chafran, L.S., Paiva, M.F., França, J.O.C., Sales, M.J.A., Dias, S.C.L., Dias, J.A., 2019. Preparation of PLA blends by polycondensation of D,L-lactic acid using supported 12-tungstophosphoric acid as a heterogeneous catalyst;. Heliyon 5, e01810.

Chen, H., Huang, M., Li, X., Liu, L., Chen, B., Wang, J., Lin, Y., 2018. Phochrodines A-D, first naturally occurring new chromenopyridines from mangrove entophytic fungus Phomopsis sp. 33. Fitoterapia 124, 103–107.

Chenera, B., West, M.L., Finkelstein, J.A., Dreyer, G.B., 1993. Total synthesis of (±)-Calanolide A, a non-nucleoside inhibitor of HIV-1 reverse transcriptase. J. Org. Chem. 58, 5605–5606.

Davidson, M.A., Mattison, D.R., Azoulay, L., Krewski, D., 2018. Thiazolidinedione drugs in the treatment of type 2 diabetes mellitus: past, present and future. Crit. Rev. Toxicol. 48, 52–108.

Engleder, M., Pichler, H., 2018. On the current role of hydratases in biocatalysis. Appl. Microbiol. Biotechnol. 102, 5841–5858.

Eskandari, K., Karami, B., 2016. Graphene oxide nanosheets-catalyzed synthesis of novel benzylbarbiturocoumarin derivatives under green conditions. Monatshefte Chem. 147, 2119–2126.

Eskandari, K., Karami, B., 2018. A nanocatalyst-assisted protocol to the synthesis of bis(pyrazolyl) methane derivatives bearing aroyl groups by the use of arylglyoxals in the presence of ZnO nanowires as a highly efficient, recyclable, and green catalyst. Can. J. Chem. 96, 377–384.

Eskandari, K., Karami, B., Khodabakhshi, S., 2014. Novel silica sodium carbonate (SSC): preparation, characterization and its first catalytic application to the synthesis of new dihydropyrano[2,3-c] pyrazoles. Catal. Commun. 54, 124–130.

Eskandari, K., Karami, B., Pourshojaei, Y., Asadipour, A., 2018a. An eco-compatible, three-component synthesis of acyl-substituted bis(pyrazolyl)methanes by employing recyclable silica sodium carbonate as an efficient and environmentally benign catalyst in aqueous medium. Monatshefte Chem. 149, 1075–1081.

Eskandari, K., Karami, B., Pourshojaei, Y., Lori-Gooini, Z., Soltanipour-Joneghani, Elham Moradi, M.-T., Asadipour, A., 2018b. Synthesis and biological evaluation of 4-hydroxychromenyl arylmethyl-6-hydroxy pyrimidine-2, 4-dione derivatives. J. Kerman Univ. Med. Sci. 25, 213–227.

Farahi, M., Karami, B., Jokar, A., Eskandari, K., 2017. An environmentally benign synthesis of pyrimidine-fused coumarin and triazole motifs via a catalytic domino reaction. Org. Prep. Proced. Int. 49, 514–524.

Fogeron, T., Todorova, T.K., Porcher, J.P., Gomez-Mingot, M., Chamoreau, L.M., Mellot-Draznieks, C., Li, Y., Fontecave, M., 2018. A bioinspired nickel(bis-dithiolene) complex as a homogeneous catalyst for carbon dioxide electroreduction. ACS Catal. 8, 2030–2038.

Friesner, R.A., Murphy, R.B., Repasky, M.P., Frye, L.L., Greenwood, J.R., Halgren, T.A., Sanschagrin, P.C., Mainz, D.T., 2006. Extra precision glide: docking and scoring incorporating a model of hydrophobic enclosure for protein-ligand complexes. J. Med. Chem. 49, 6177–6196.

Fukutake, T., Wada, K., Liu, G.C., Hosokawa, S., Feng, Q., 2018. Striking effects of a titania support on the low-temperature activities of Ir catalysts for the dehydrogenative synthesis of benzimidazole and indole. Catal. Today 303, 235–240.

Guo, R.Y., An, Z.M., Mo, L.P., Wang, R.Z., Liu, H.X., Wang, S.X., Zhang, Z.H., 2013. Meglumine: a novel and efficient catalyst for one-pot, three-component combinatorial synthesis of functionalized 2-amino-4H-pyrans. ACS Comb. Sci. 15, 557–563.

Gupta, N., Roy, T., Ghosh, D., Abdi, S.H.R., Kureshy, R.I., Khan, N.U.H., Bajaj, H.C., 2015. Ordered short channel mesoporous silica modified with 1,3,5-triazine-piperazine as a versatile recyclable basic catalyst for cross-aldol, Knoevenagel and conjugate addition reactions with isatins. RSC Adv. 5, 17843–17850.

Habibi, A., Eskandari, K., Alizadeh, A., 2012. Synthesis and dynamic NMR study of new stable ylides derived from the reaction of triphenylphosphine, dialkyl acetylenedicarboxylates, and 5-ACYL meldrums acid. Phosphorus Sulfur 187, 1109–1117.

Karami, B., Eskandari, K., Azizi, M., 2013a. Tungstate sulfuric acid (TSA): a green and highly efficient catalyst for novel and known polysubstituted imidazoles synthesis. Lett. Org. Chem. 10, 722–732.

Karami, B., Eskandari, K., Gholipour, S., Jamshidi, M., 2013b. Facile and rapid synthesis of 9-aryl 1,8-dioxoöctahydroxanthenes derivatives using tungstate sulfuric acid. Org. Prep. Proced. Int. 45, 220–226.

Karami, B., Eskandari, K., Khodabakhshi, S., 2012. One-pot, three component approach to synthesis of multipart fused heterocyclic compounds: synthesis of fused pyran-2-ones. Arkivoc 2012, 76–84.

Karami, B., Eskandari, K., Khodabakhshi, S., Hoseini, S.J., Hashemian, F., 2013c. Green synthesis of three substituted methane derivatives by employing ZnO nanoparticles as a powerful and recyclable catalyst. RSC Adv. 3, 23335.

Karami, B., Zare, Z., Eskandari, K., 2013d. Molybdate sulfonic acid: preparation, characterization, and application as an effective and reusable catalyst for octahydroxanthene-1,8-dione synthesis. Chem. Pap. 67, 145–154.

Khalili, S.S., Dehghani, H., 2016. Ca-doped CuS/graphene sheet nanocomposite as a highly catalytic counter electrode for improving quantum dot-sensitized solar cell performance. RSC Adv. 6, 10880–10886.

Kitt, J., Irons, R., Al-Obaidi, M., Missouris, C., 2015. A case of donepezil-related torsades de pointes. BMJ Case Rep. 2015, 1–3.

Kocięcka, P., Czeluśniak, I., Panek, J., Szymańska-Buzar, T., 2018. Unusual product formation in tungsten(0)-catalysed reactions of propargylic alcohols and secondary amines: hydroamination and the construction of the tetrahydrofuran ring. Mol. Catal. 455, 23–31.

Lee, J., Lee, D.G., Rodriguez, J.P., Park, J.Y., Cho, E.J., Jacinto, S.D., Lee, S., 2018. Determination of flavonoids in Acer okamotoanum and their aldose reductase inhibitory activities. Hortic. Environ. Biotechnol. 59, 131–137.

Li, H., McRae, L., Elezzabi, A.Y., 2018a. Solution-processed interfacial PEDOT:PSS assembly into porous tungsten molybdenum oxide nanocomposite films for electrochromic applications. ACS Appl. Mater. Interfaces 10, 10520–10527.

Li, P., Liu, Y., Wang, L., Xiao, J., Tao, M., 2018b. Copper(II)-Schiff base complex-functionalized polyacrylonitrile fiber as a green efficient heterogeneous catalyst for one-pot multicomponent syntheses of 1,2,3-triazoles and propargylamines. Adv. Synth. Catal. 360, 1673–1684.

Li, Y., Du, B., Wang, X., Shi, D., Tu, S., 2006. Synthesis of 2-amino-4-aryl-7,7-dimethyl-5-oxo-4H-5,6,7,8- tetrahydrobenzo[b]pyran derivatives in ionic liquid medium. J. Heterocycl. Chem. 43, 685–688.

Liu, H. ran, Men, X., Gao, X. hui, Liu, L. bo, Fan, H. qun, Xia, X. hua, Wang, Q. an, 2018a. Discovery of potent and selective acetylcholinesterase (AChE) inhibitors: acacetin 7-O-methyl ether Mannich base derivatives synthesised from easy access natural product naringin. Nat. Prod. Res. 32, 743–747.

Liu, M., Liu, W., Pang, L., Teng, H., Fang, S., Wei, Z., 2018b. Ultrashort pulse generation in mode-locked erbium-doped fiber lasers with tungsten disulfide saturable absorber. Opt. Commun. 406, 72–75.

Maleki, A., Ghamari, N., Kamalzare, M., 2014. Chitosan-supported Fe3O4 nanoparticles: a magnetically recyclable heterogeneous nanocatalyst for the syntheses of multifunctional benzimidazoles and benzodiazepines. RSC Adv. 4, 9416–9423.

Maleki, B., 2016a. Green synthesis of bis-coumarin and dihydropyrano[3,2-c]chromene derivatives catalyzed by o-benzenedisulfonimide. Org. Prep. Proced. Int. 48, 303–318.

Maleki, B., 2016b. One-pot synthesis of some2-amino-4H-benzo[g]chromenes. Org. Prep. Proced. Int. 48, 81–87.

Maleki, B., Babaee, S., Tayebee, R., 2015. Zn (L-proline) 2 as a powerful and reusable organometallic catalyst for the very fast synthesis of 2-amino-4H-benzo chromene derivatives under solvent-free. Appl. Organomet.

Maleki, B., Sheikh, S., 2015a. One-pot synthesis of 2-Amino-2-chromene and 2-Amino-3-cyano-4H-pyran derivatives promoted by potassium fluoride. Org. Prep. Proced. Int. 47, 368–378.

Maleki, B., Sheikh, S., 2015b. Nano polypropylenimine dendrimer (DAB-PPI-G_1): as a novel nano basic-polymer catalyst for one-pot synthesis of 2-amino-2-chromene derivatives. RSC Adv. 5, 42997–43005.

Mehrabi, F., Pourshojaei, Y., Moradi, A., Sharifzadeh, M., Khosravani, L., Sabourian, R., Rahmani-Nezhad, S., Mohammadi-Khanaposhtani, M., Mahdavi, M., Asadipour, A., Rahimi, H.R., Moghimi, S., Foroumadi, A., 2017. Design, synthesis, molecular modeling and anticholinesterase activity of benzylidene-benzofuran-3-ones containing cyclic amine side chain. Future Med. Chem. 9, 659–671.

Mohamed, L.W., Abuel-Maaty, S.M., Mohammed, W.A., Galal, M.A., 2018. Synthesis and biological evaluation of new oxopyrrolidine derivatives as inhibitors of acetyl cholinesterase and β amyloid protein as anti – Alzheimer's agents. Bioorg. Chem. 76, 210–217.

Patra, A., Mahapatra, T., 2010. Synthesis of tetrahydrobenzo [b] pyran derivatives catalysed by Aliquat® 336 in water under microwave irradiation. J. Chem. Res. 34, 689–693.

Pourshojaei, Yaghoub, Jadidi, M.H., Eskandari, K., Foroumadi, A., Asadipour, A., 2018a. An eco-friendly synthesis of 4-aryl-substituted pyrano-fuzed coumarins as potential pharmacological active heterocycles using molybdenum oxide nanoparticles as an effective and recyclable catalyst. Res. Chem. Intermed. 44, 4195–4212.

Pourshojaei, Y., Nikzad, M., Eskandari, K., Darijani, M.-H., Hassanzadeh, A., Faghih-Mirzaei, E., Asadipour, A., 2018b. Ultrasound-assisted and efficient knoevenagel condensation reaction catalyzed by silica sodium carbonate nanoparticles. Croat. Chem. Acta 91, 19–28.

Pullur Anil Kumar, H.P.H., 2010. Synthesis and dispersion of dendrimer-encapsulated Pt nanoparticles on γ-Al2O3 for the reduction of NO x by methane. Catal. Lett. 136, 177–184.

Rahmani-Nezhad, S., Khosravani, L., Saeedi, M., Divsalar, K., Firoozpour, L., Pourshojaei, Y., Sarrafi, Y., Nadri, H., Moradi, A., Mahdavi, M., Shafiee, A., Foroumadi, A., 2015. Synthesis and evaluation of coumarin-resveratrol hybrids as 15-lipoxygenaze inhibitors. Synth. Commun. 45, 751–759.

Rong, L., Li, X., Wang, H., Shi, D., Tu, S., Zhuang, Q., 2006. Efficient synthesis of tetrahydrobenzo[b]pyrans under solvent-free conditions at room temperature. Synth. Commun. 36, 2363–2369.

Saidi, M.R., Pourshojaei, Y., Aryanasab, F., 2009. Highly efficient Michael addition reaction of amines catalyzed by silica-supported aluminum chloride. Synth. Commun. 39, 1109–1119.

Uruş, S., Karabörk, M., Köksal, H., 2018. Synthesis, characterization and solid-phase extraction properties of novel bis(diazo-azomethine) ligands supported on mesoporous silica. Appl. Organomet. Chem. 32.

Waghmare, S.D., Jadhav, V.V., Shaikh, S.F., Mane, R.S., Rhee, J.H., O'Dwyer, C., 2018. Sprayed tungsten-doped and undoped bismuth ferrite nanostructured films for reducing and oxidizing gas sensor applications. Sensors Actuators, A Phys. 271, 37–43.

Wang, X.S., Shi, D.Q., Tu, S.J., Yao, C.S., 2003. A convenient synthesis of 5-oxo-5,6,7,8-tetrahydro-4H-benzo-[b]-pyran derivatives catalyzed by KF-alumina. Synth. Commun. 33, 119–126.

Ye, R., Zhukhovitskiy, A.V., Kazantsev, R.V., Fakra, S.C., Wickemeyer, B.B., Toste, F.D., Somorjai, G.A., 2018. Supported Au nanoparticles with N -heterocyclic carbene ligands as active and stable heterogeneous catalysts for lactonization. J. Am. Chem. Soc. 140, 4144–4149.

Zhai, Y., Zhao, J., Di, X., Di, S., Wang, B., Yue, Y., Sheng, G., Lai, H., Guo, L., Wang, H., Li, X., 2018. Carbon-supported perovskite-like CsCuCl3nanoparticles: a highly active and cost-effective heterogeneous catalyst for the hydrochlorination of acetylene to vinyl chloride. Catal. Sci. Technol. 8, 2901–2908.